

PAPER

Surface Height Change Estimation Method Using Band-Divided Coherence Functions with Fully Polarimetric SAR Images

Ryo OYAMA[†], *Nonmember*, Shouhei KIDERA^{†a)}, and Tetsuo KIRIMOTO[†], *Members*

SUMMARY Microwave imaging techniques, in particular, synthetic aperture radar (SAR), are promising tools for terrain surface measurement, irrespective of weather conditions. The coherent change detection (CCD) method is being widely applied to detect surface changes by comparing multiple complex SAR images captured from the same scanning orbit. However, in the case of a general damage assessment after a natural disaster such as an earthquake or mudslide, additional about surface change, such as surface height change, is strongly required. Given this background, the current study proposes a novel height change estimation method using a CCD model based on the Pauli decomposition of fully polarimetric SAR images. The notable feature of this method is that it can offer accurate height change beyond the assumed wavelength, by introducing the frequency band-divided approach, and so is significantly better than InSAR based approaches. Experiments in an anechoic chamber on a 1/100 scaled model of the X-band SAR system, show that our proposed method outputs more accurate height change estimates than a similar method that uses single polarimetric data, even if the height change amount is over the assumed wavelength.

key words: *synthetic aperture radar (SAR), fully polarimetric analysis, coherent change detection (CCD), multiply band-divided SAR images, height change estimation*

1. Introduction

Synthetic aperture radar (SAR) is the most powerful imaging tool for microwave remote sensing systems, which is able to estimate the structure of terrain surfaces regardless of lighting or weather conditions [1], [2]. A notable feature of SAR image is that these complex-valued images, in particular, their phase component, can be exploited to analyze the height or structural features of targets. To conduct this, the coherent change detection (CCD) method, one of the most cutting edge derivative techniques of SAR, has been developed [3], [4]. The concept of CCD is simply based on local spatial correlation between sequential complex SAR images obtained through observations of the same region at different times. There are various extensions of the original CCD method, such as more accurate change detection using the phase of the coherence function [5]. However, traditional CCD techniques were designed only for change detection, and so failed to address height change measurements. Height change is strongly required to judge if a road is suitable for motor vehicle use following a natural disaster, such as huge earthquake or deadly mudslide.

Interferometric SAR (InSAR) is one of the promising solutions for extracting height information from complex SAR images, which is based on the phase interferometry of plural SAR images obtained from different scanning orbits [6], [7]. However, InSAR often suffers from inaccuracy caused by difficulty of phase unwrapping problem and is not designed for extracting the temporal height change, basically. There are various derivation techniques for InSAR, such as the polarimetric approach (PolInSAR) [8], which classifies a target according to the characteristic polarization of the received signal; and a method [9] based on the differential SAR Interferometry (DinSAR), which employs the likelihood function and frequency diversity to unwrap a phase distribution. However, this type of technique has a significant drawback due to phase wrapping because the obtained height is relative to a reference point, and thus, in the case of great height changes in spatially narrow areas, this method fails to output the correct relative height distribution. To overcome such unwrapping problem, the intensity based offset tracking have been developed by using cross-correlation of PolSAR images [10]. Nonetheless, since the InSAR-based techniques described above were developed for height estimation method, they are incapable of detecting change because they assume the temporal invariance of the target surface.

As a suitable approach for this issue, we have already proposed a method to estimate the height change with a CCD model [11], in particular, one that employs multiple band-divided SAR images and their coherence functions with associated phases. To accurately reconstruct the height change, this method focuses on the phase characteristics of each center frequency and resolves ambiguities by employing a multiple non-linear regression scheme. It enhances robustness against phase fluctuations by employing, rather than spatial averaging, a type of frequency averaging scheme. Thus, it can maintain the accuracy of height change estimation without degrading the spatial resolution of the estimation, and thus is also suitable for detecting temporal change in the target surface. However, this method is oriented to the single polarimetric case. It should be appropriately extended to the fully polarimetric case to enhance the height change estimation accuracy.

According to the above background, this study introduces an extension of the height change estimation method to fully polarimetric data. There are various studies on fully polarimetric SAR analysis that focus on structural recognition of features, such as the ground surface, paddy fields,

Manuscript received February 21, 2017.

Manuscript revised May 9, 2017.

Manuscript publicized May 19, 2017.

[†]The authors are with Graduate School of Informatics and Engineering, The University of Electro-Communications, Chofu-shi, 182-8585 Japan.

a) E-mail: kidera@ee.uec.ac.jp

DOI: 10.1587/transcom.2017EBP3067

forests, and artificial buildings [12], [13]. As the most useful tool for this analysis, Pauli decomposition has been widely applied to determine the dominant scattering components such as surface scattering, double-bounced scattering, and volume scattering [14], [15]. Furthermore, this study adopts the Pauli decomposition for height change estimation, which enables us to extract the dominant, in particular higher SNR components. A notable feature of this method is its applicability to the beyond-the-wavelength height change situations, by using the band-divided and synthesizing approach, and should be a significant advantage over InSAR-based estimation. The experimental data, assuming a 1/100 scaledown model of the X-band SAR system, validate that our proposed index significantly enhances the accuracy of the height change estimation compared with that obtained by the same method using single polarimetric data.

2. System Model

Figure 1 shows the observation geometry. The target is assumed to have a rough surface around the $z = 0$ plane, and the propagation speed of the microwaves is a known constant and denoted as c . Mono-static radar is used to correct a set of scans along the x axis line, located at $y = 0, z = z_0$. The off-nadir angle is denoted by θ . Each antenna receives the complex-valued reflection signal $s(x; f)$ at each frequency f , where the signal is swept through a finite frequency range. The height of the target surface is changed as $\Delta z_{\text{true}}(x, y)$ between the first and second observations. The two linear polarizations are assumed to be vertical (denoted by V) and horizontal (denoted by H) with respect to the transmitting and receiving antennas. Following this, fully polarimetric data characterized by VV, VH, HV and HH are obtained. For example, VH denotes horizontal polarization in transmitting and vertical polarization in receiving and assumes the reciprocity as $HV = VH$. The polarimetric SAR complex image, focused on the $z = 0$ plane at the p th observation, is defined as $S_p^{ij}(x, y)$, where the subscripts i and j denote H or V, and p denotes 1 or 2. In this manner, a scattering vector \mathbf{X}_p is defined as follows:

$$\mathbf{X}_p(x, y) \equiv \left[S_p^{\text{HH}}(x, y), \sqrt{2}S_p^{\text{HV}}(x, y), S_p^{\text{VV}}(x, y) \right]^T \quad (1)$$

The normal coherence function $\gamma(x, y)$ between the complex SAR images $S_1^{ij}(x', y')$ and $S_2^{ij}(x', y')$ is defined as follows:

$$\begin{aligned} \gamma^{ij}(x, y) = & \frac{\iint_{\Omega(x, y)} S_1^{ij}(x' - x, y' - y) S_2^{ij}(x' - x, y' - y)^* dx' dy'}{\sqrt{\iint_{\Omega(x, y)} |S_1^{ij}(x' - x, y' - y)|^2 dx' dy'}} \\ & \times \frac{1}{\sqrt{\iint_{\Omega(x, y)} |S_2^{ij}(x' - x, y' - y)|^2 dx' dy'}}, \quad (2) \end{aligned}$$

where $*$ denotes a complex conjugate and $\Omega(x, y)$ denotes

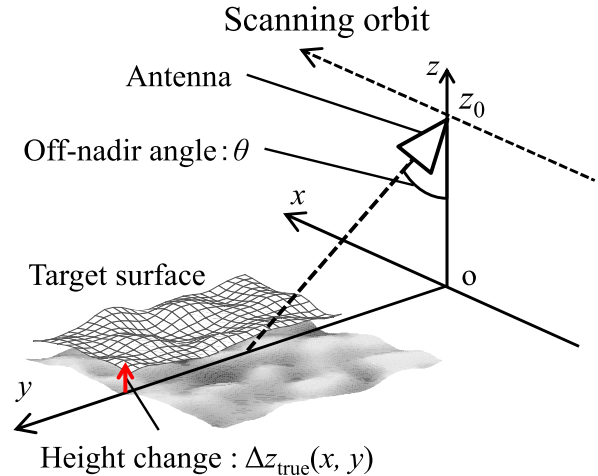


Fig. 1 Observation geometry.

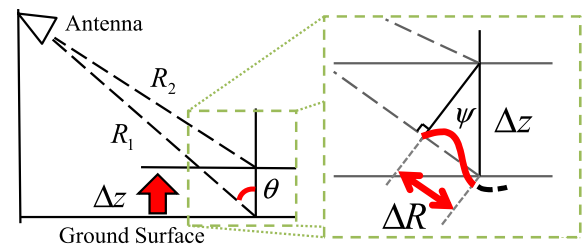


Fig. 2 Geometrical relationship between the phase difference and height change amount.

the size of the correlation. Clearly, $0 \leq |\gamma^{ij}(x, y)| \leq 1$ holds true.

Under the assumption that the target surface moves along the z axis, the height change $\Delta z^{ij}(x, y)$ can be calculated from the phase of the coherence function $\gamma^{ij}(x, y)$,

$$\Delta z^{ij}(x, y) \approx -\frac{c}{4\pi f_c \cos \theta(x, y)} \psi^{ij}(x, y), \quad (3)$$

where $\psi^{ij}(x, y)$ denotes the phase of $\gamma^{ij}(x, y)$ and f_c is the center frequency of the transmitted signal, and $\theta(x, y)$ is the off nadir angle averaged over all antenna locations of observations. Figure 2 shows the geometrical relationship between the height change and off-nadir angle. Note that there should be ambiguity in determining the actual height change due to the phase of the coherence function. The amount of this ambiguity for the center frequency f_c is calculated as follows:

$$\Delta z_{\text{amb}} = \frac{c}{2f_c \cos \theta(x, y)}, \quad (4)$$

which makes height change estimation difficult.

3. Conventional Method

This section introduces the conventional method as one approach for the height change estimation using the CCD model which employs multiple band-divided SAR images and their

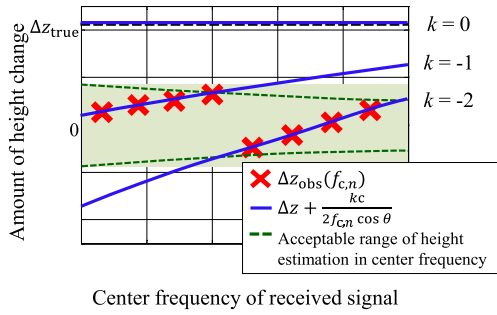


Fig. 3 Conventional fitting approach for height change estimation with multiple frequency bands, assuming single polarimetric data.

coherence functions [11]. This method focuses on the frequency characteristics of the multiple phases obtained by the multiple coherence functions to avoid ambiguity errors in the height change estimation. First, the multiple band-divided data are generated from the received signal, with each having the same frequency band but a different center frequency denoted as $f_{c,n}$ ($n = 1, 2, \dots, N$), where N is the total number of the divided frequency bands. Second, the SAR images of each observation are generated for each frequency band as $S_p(x, y; f_{c,n})$, where $p = 1, 2$ denotes the observation number. Third, the coherence functions between $S_1(x, y; f_{c,n})$ and $S_2(x, y; f_{c,n})$ are calculated for each frequency band using Eq. (2). Using the phase of the coherence functions, height change $\Delta z_{\text{obs}}(x, y; f_{c,n})$ is calculated as

$$\Delta z_{\text{obs}}(x, y; f_{c,n}) = -\frac{c}{4\pi f_{c,n} \cos \theta} \psi(x, y; f_{c,n}), \quad (5)$$

where $\psi(x, y; f_{c,n})$ denotes the phase of the coherence function for n th frequency band. To resolve the ambiguity of height change estimation, the optimum amount of height change $\hat{\Delta z}(x, y)$ is calculated as follows:

$$\hat{\Delta z}_{\text{single}}(x, y) = \arg \min_{|\Delta z| \leq \Delta z_{\text{max}}} \sum_{n=1}^N \min_{k \in \mathbf{Z}} \left| \Delta z_{\text{obs}}(x, y; f_{c,n}) - \left(\Delta z + \frac{kc}{2f_{c,n} \cos \theta} \right) \right|^2, \quad (6)$$

where Δz_{max} denotes the investigating range of height estimation, which is set to sufficiently large value. Figure 3 shows the fitting approach of Eq.(6). In this figure, the investigating index Δz correctly fits into the actual value Δz_{true} because the curved line is completely adjusted to $\Delta z_{\text{obs}}(f_{c,n})$. Although the band-divided data are not completely independent from each other, this method can enhance the robustness of phase fluctuations by employing multiple frequency data points. However, this method is oriented only to the single polarimetric case.

4. Proposed Method

This section introduces the principle and methodology of the proposed method. Our proposed method appropriately extends the conventional method (described in Sect.3) to

the fully polarimetric case, where each Pauli component is assessed for height change estimation as follows. First, a received signal for each polarimetric combination, HH, HV and VV, is divided into multiple bands in the frequency domain, where each band has the same bandwidth but a different center frequency, denoted as $f_{c,n}$. Second, the fully polarimetric SAR images at the p th observation are generated for each frequency band using $S_p^{ij}(x, y; f_{c,n})$, where the superscript i and j denote H or V. Next, each band-divided polarimetric SAR image is decomposed into the Pauli scattering vector $\mathbf{k}_p(x, y; f_{c,n})$ as follows:

$$\mathbf{k}_p(x, y; f_{c,n}) \equiv \frac{1}{\sqrt{2}} \begin{bmatrix} S_p^{\text{HH}}(x, y; f_{c,n}) + S_p^{\text{VV}}(x, y; f_{c,n}) \\ S_p^{\text{HH}}(x, y; f_{c,n}) - S_p^{\text{VV}}(x, y; f_{c,n}) \\ 2S_p^{\text{HV}}(x, y; f_{c,n}) \end{bmatrix}, \quad (7)$$

where the first, second, and third rows of $\mathbf{k}_p(x, y; f_{c,n})$ are usually regarded as the surface, double and volume scattering components, respectively. Here, a spatial gap because of layover effect between $\mathbf{k}_1(x, y; f_{c,n})$ and $\mathbf{k}_2(x, y; f_{c,n})$ are compensated for each SAR image by evaluating the local cross-correlation functions between the 1st and 2nd observed SAR images. Next, let $\gamma(x, y; f_{c,n}, r)$ and $\psi(x, y; f_{c,n}, r)$ denote the coherence function and its phase between the r th row components of $\mathbf{k}_1(x, y; f_{c,n})$ and $\mathbf{k}_2(x, y; f_{c,n})$ after the spatial gap compensation. When $|\psi(x, y; f_{c,n}, r)| \leq \pi$ holds, the height change $\Delta z_{\text{obs}}(x, y; f_{c,n}, r)$ is directly calculated as follows:

$$\Delta z_{\text{obs}}(x, y; f_{c,n}, r) = -\frac{c}{4\pi f_{c,n} \cos \theta} \psi(x, y; f_{c,n}, r). \quad (8)$$

However, when $|\psi(x, y; f_{c,n}, r)| > \pi$ holds, the ambiguity errors should be considered. To avoid such ambiguity errors in the height change estimation, this method introduces the evaluation function as follows:

$$f(\Delta z; x, y, r) = \sum_{n=1}^N \min_{k \in \mathbf{Z}} \left| \Delta z_{\text{obs}}(x, y; f_{c,n}, r) - \left(\Delta z + \frac{kc}{2f_{c,n} \cos \theta} \right) \right|^2. \quad (9)$$

Next, the optimal height change amount $\tilde{\Delta z}(x, y; r)$ for each of the r th Pauli components is determined as follows:

$$\tilde{\Delta z}(x, y; r) = \arg \min_{|\Delta z| \leq \Delta z_{\text{max}}} f(\Delta z; x, y, r), \quad (10)$$

where Δz_{max} denotes the range of height estimation. Then, the optimal Pauli component \hat{r} for height change estimation is determined as;

$$\hat{r} = \arg \min_r f(\tilde{\Delta z}(x, y; r); x, y, r). \quad (11)$$

Finally, the height change $\hat{\Delta z}_{\text{full}}(x, y)$, which considers fully polarimetric data is calculated as follows:

$$\hat{\Delta z}_{\text{full}}(x, y) = \tilde{\Delta z}(x, y; \hat{r}) \quad (12)$$

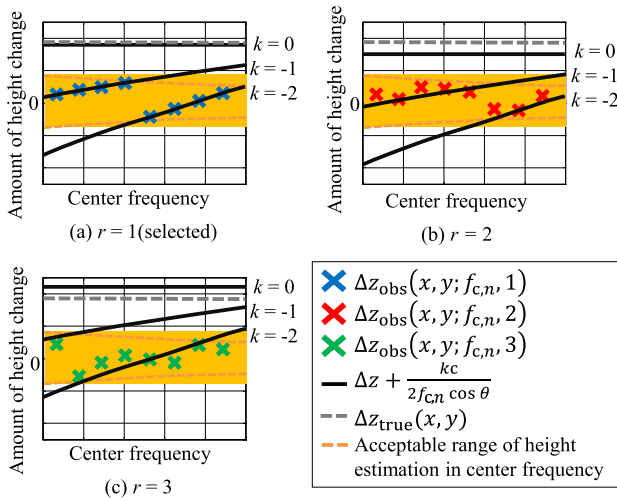


Fig. 4 Fitting approach for height change estimation with each Pauli component.

This procedure is a natural extension of the single polarimetric case method as described in Sect. 3. Figure 4 shows the fitting approach of each Pauli component expressed in Eq. (9) for cases when surface scattering is dominant, in particular, when the 1st Pauli component is higher than other components. Because the SNR of the 1st Pauli scattering component also becomes relatively high, there are less fluctuations in observed data points in case (a), and the evaluation function is considered to be at a minimum. In other words, the proposed method can select the optimal estimation for the height change by considering the dominant scattering phenomena.

The actual procedure of the proposed method is summarized as follows.

- Step 1)** For each center frequency $f_{c,n}$, Pauli scattering vector $\mathbf{k}_1(x, y; f_{c,n})$ and $\mathbf{k}_2(x, y; f_{c,n})$ are obtained by band-divided fully polarimetric SAR images.
- Step 2)** Coherence functions $\gamma(x, y; f_{c,n}, r)$ are calculated for each Pauli component and divided frequency band after the spatial gap compensation. The phase $\psi(x, y; f_{c,n}, r)$ is extracted.
- Step 3)** For each row of Pauli vectors, the height change amount $\Delta z_{\text{obs}}(x, y; f_{c,n}, r)$ is estimated from $\psi_r(x, y; f_{c,n})$ in Eqs. (10) and (11).
- Step 4)** The optimal height change amount $\hat{\Delta z}_{\text{full}}(x, y)$ is determined using Eq. (12).

Figure 5 shows the flowchart of the proposed method.

5. Experimental Validation

This section describes the performance evaluation for each method using the experimental data. This experiment assumes a 1/100 scaled-down model of an X-band SAR system for the observation geometry and spatial resolution, except for the center frequency. Figure 6 shows the setup of the experiment. The 3 dB beam width of each horn antenna is

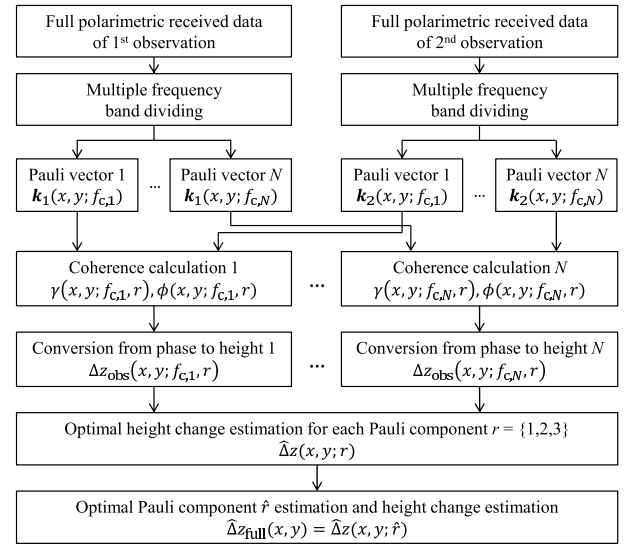


Fig. 5 Flowchart of the proposed method.

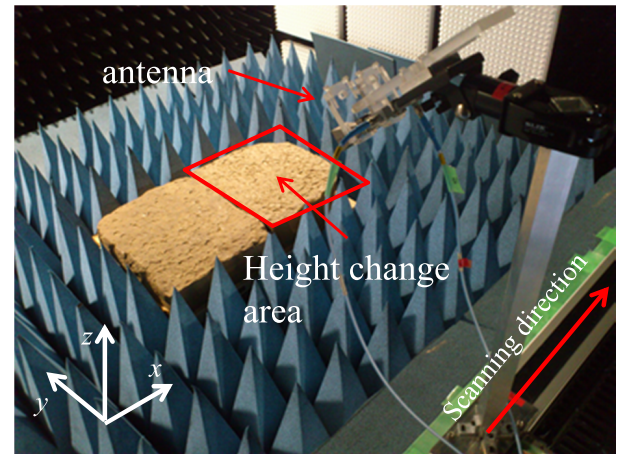


Fig. 6 Experimental setup.

27 degrees, and the interval between the transmitting and receiving antennas is 48 mm. The set of transmitting and receiving antennas is scanned for the range of $-800 \text{ mm} \leq x \leq 800 \text{ mm}$, where $y = 0 \text{ mm}$ and $z_0 = 900 \text{ mm}$ holds true. On the transmitter side, a 20 dB amplifier is inserted to obtain a sufficient echo from the targets. Reflection data are obtained by VNA (Vector Network Analyzer), where the frequency is swept from $f_{\text{min}} = 26 \text{ GHz}$ to $f_{\text{max}} = 40 \text{ GHz}$ at 10 MHz intervals. The off-nadir angle is 50.0 degree. Two clay objects with rough surfaces (roughness is approximately $\pm 1 \text{ mm}$) are neighbored along the x-axis, assumed to simulate the ground surface. The width, depth and thickness of each clay target are 400 mm, 500 mm, and 100 mm, respectively. The number of divided frequency bands N is 7, where each bandwidth of the received signal is 8 GHz and the interval of the center frequency is 1 GHz. The theoretical range resolutions before and after band dividing are 14.0 mm and 24.5 mm, respectively. The theoretical azimuth resolution is approximately 12.5 mm, regardless of band division. One clay

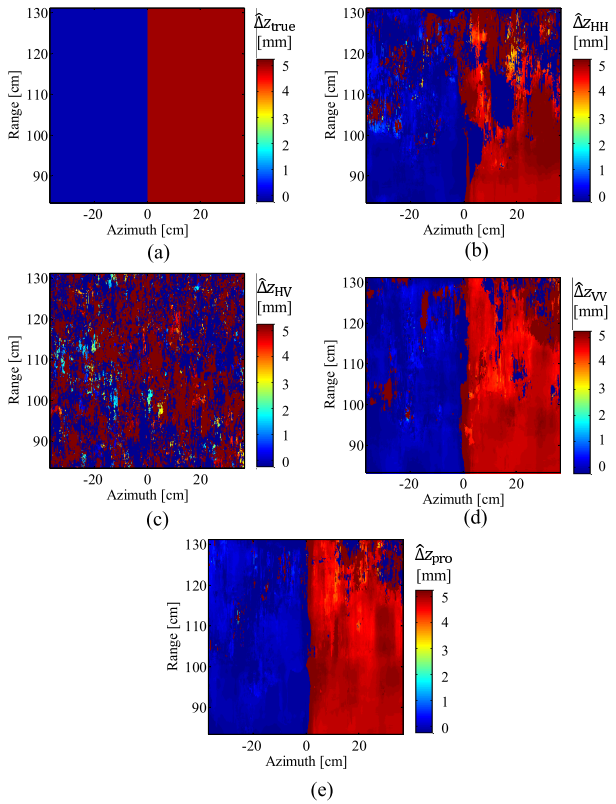


Fig. 7 Distribution of height change at Case 1 (height change is 5 mm) ((a): Actual, (b): Estimated by S_{HH} , (c): Estimated by S_{HV} (d): Estimated by S_{VV} (e): Estimated by the proposed method).

target located $x \geq 0$ is uniformly lifted as $\Delta z_{true}(x, y)$ mm following the first observation. We consider the three height change cases as follows.

Case 1 Height change is within λ_c as:

$$\Delta z_{true}(x, y) = \begin{cases} 5\text{mm}, & (x \geq 0) \\ 0\text{mm}, & (x < 0) \end{cases} \quad (13)$$

Case 2 Height change is almost same as λ_c as:

$$\Delta z_{true}(x, y) = \begin{cases} 10\text{mm}, & (x \geq 0) \\ 0\text{mm}, & (x < 0) \end{cases} \quad (14)$$

Case 3 Height change is beyond λ_c as:

$$\Delta z_{true}(x, y) = \begin{cases} 20\text{mm}, & (x \geq 0) \\ 0\text{mm}, & (x < 0) \end{cases} \quad (15)$$

The white Gaussian components are added to the received signal in the frequency domain to simulate lower SNR situations. For example, at Case 1, the SNRs of HH, HV and VV polarization are 27, 12, 28 dB, respectively. On the other hand, the SNRs of 1st, 2nd and 3rd component of Pauli vector are 31, 20, 12 dB, respectively. This SNR differences means that the highest SNR component is regarded as 1st component of Pauli vector, namely, the surface scattering component is dominant in this case, which is compatible to the assumed situation. Figure 7 shows

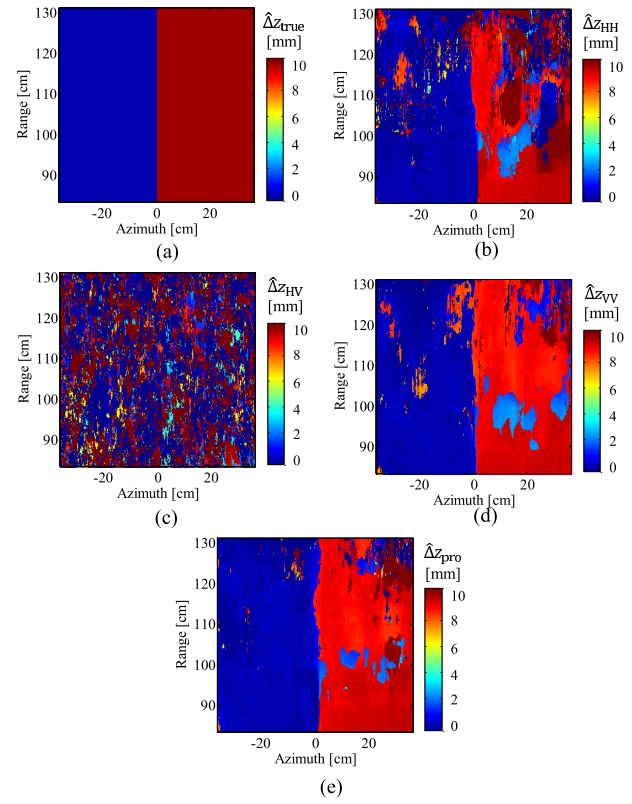


Fig. 8 Distribution of height change at Case 2 (height change is 10 mm). ((a): Actual, (b): Estimated by S_{HH} , (c): Estimated by S_{HV} (d): Estimated by S_{VV} (e): Estimated by the proposed method).

the height change estimation results in Case 1, obtained by each single polarimetric data and the proposed method. As shown in this figure, the VV and the proposed mixing component offers accurate estimation, while the HV component provide almost random height change estimation, which is due to the lowest SNR component. Note that, the proposed method could offer the best estimation by comparing the VV and HH based height change estimation results through Pauli decomposition (comparing the cost function in each pixel), and cover the largest area with high accuracy. Figures 8 and 9 show the height change estimation results in Case 2 and Case 3, respectively, obtained by each single polarimetric data and the proposed method. While Fig. 8 (Case 2) shows that the proposed method retains accurate estimations as well as that obtained in Case 1, in the Case 3, our proposed method and other components based estimation suffer from accuracy degradation compared with those obtained in Case 1 and Case 2. This is due to the fact that the optimal solution around here does not reach the global optimal, which should be addressed with in our future work by adding the regularization term to the cost function. However, the proposed method has a significant advantage from the InSAR or DInSAR based estimation, where the phase unwrapping problem would offer an estimation ambiguity in height change estimation, especially in Case 3.

For quantitative analysis of the height change estimation, the ambiguity resolution probability is introduced as

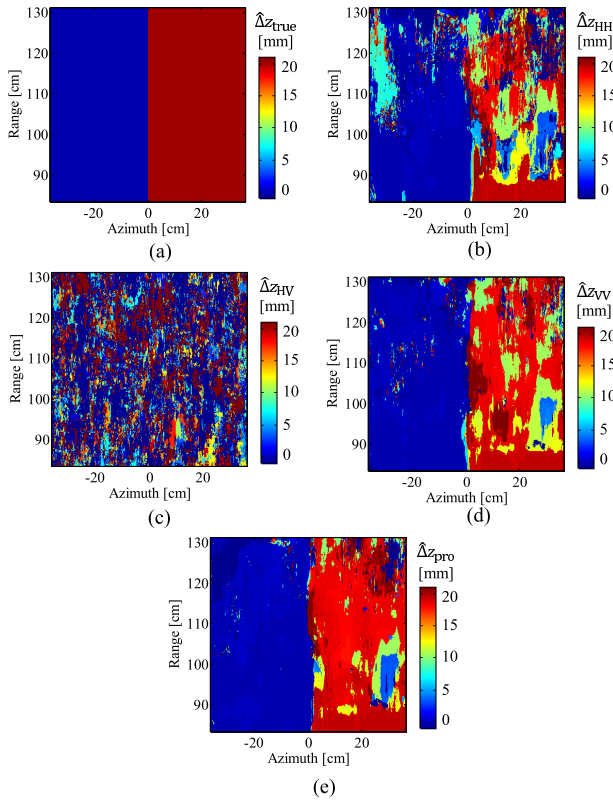


Fig. 9 Distribution of height change at Case 3 (height change is 20 mm). ((a): Actual, (b): Estimated by S_{HH} , (c): Estimated by S_{HV} (d): Estimated by S_{VV} (e): Estimated by the proposed method).

the ratio of the number of pixels satisfying the following equation to the total number of pixels.

$$|\Delta z_{true}(x, y) - \hat{\Delta z}_{est}(x, y)| < \frac{c}{4f_c \cos \theta}, \quad (16)$$

where $f_c = (f_{min} + f_{max})/2$ holds true. Figures 10, 11 and 12 show the probability of ambiguity resolution, the median error and inter quartile range (IQR) of height change estimations at Case 1, Case 2 and Case 3, respectively, where the IQR denotes the difference between 75th (3rd quartile) and 25th (1st quartile) percentiles of statical values.

These figures demonstrate that the proposed method enhances the ambiguity resolution probability, which leads to less median error or IQR quantities compared with those obtained by the method in Sect. 3, which uses single polarization data, even in the case that the height change amount is beyond the center wavelength. This is because the proposed method, based on Pauli decomposition, can select the dominant scattering effect, surface, double-bounce, and volume scattering efficiently, and eliminates lower SNR components. As previously mentioned, in these cases, the surface scattering component, the 1st component of Eq. (7) is actually dominant and retains the highest SNR compared with other components.

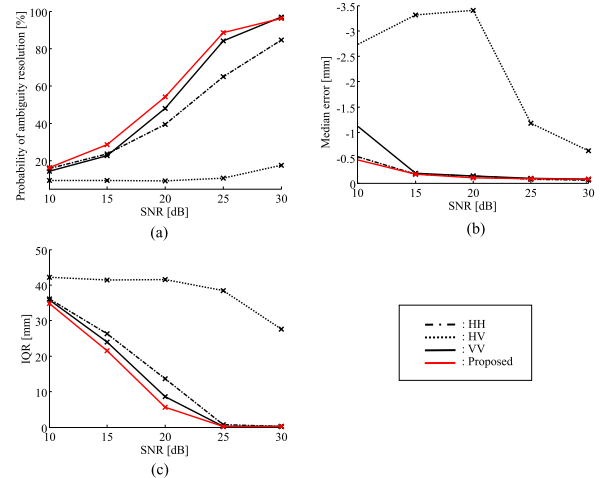


Fig. 10 Statistical evaluation for height change estimation errors at Case 1 ((a): Probability of ambiguity resolution, (b): Median, and (c): IQR).

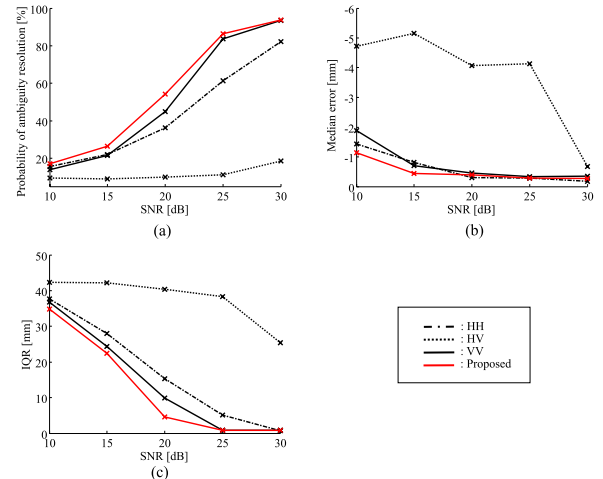


Fig. 11 Statistical evaluation for height change estimation errors at Case 2 ((a): Probability of ambiguity resolution, (b): Median, and (c): IQR).

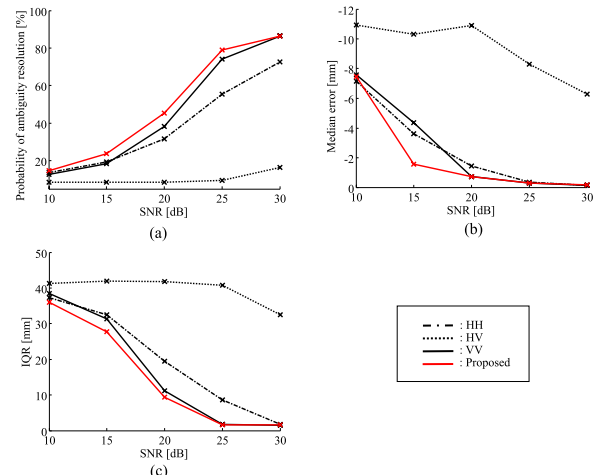


Fig. 12 Statistical evaluation for height change estimation errors at Case 3 ((a): Probability of ambiguity resolution, (b): Median, and (c): IQR).

6. Conclusion

This study proposed an accurate height change estimation method that exploits the phases of the coherence functions obtained from multiple band-divided and fully polarimetric SAR images. The ambiguities for the height change estimation are appropriately eliminated by the multi-frequency band based approach, and more high-value SNR components are extracted through the Pauli decomposition process. The results of a scaled-down experiment in an anechoic chamber, verify that the proposed method significantly enhances the estimation accuracy of surface height change when compared with methods using single polarization, even in the case that the height change amount is beyond the center wavelength.

References

- [1] W.M. Brown, "Synthetic aperture radar," *IEEE Trans. Aerosp. Electron. Syst.*, vol.AES-3, no.2, pp.217–229, March 1967.
- [2] L.M.H. Ulander, H. Hellsten, and G. Stenstrom, "Synthetic-aperture radar processing using fast factorized back-projection," *IEEE Trans. Aerosp. Electron. Syst.*, vol.39, no.3, pp.760–776, July 2003.
- [3] R. Touzi, A. Lopes, J. Bruniquel, and P.W. Vachon, "Coherence estimation for SAR imagery," *IEEE Trans. Geosci. Remote Sens.*, vol.37, no.1, pp.135–149, Jan. 1999.
- [4] G. Franceschetti and R. Lanari, *Synthetic Aperture Radar Processing*, pp.185–195, CRC Press, New York, 1999.
- [5] T. Hoshino, S. Kidera, and T. Kirimoto, "Accurate surface change detection method using phase of coherence function on SAR imagery," *IEICE Trans. Commun.*, vol.E95-B, no.1, pp.263–270, Jan. 2012.
- [6] P.A. Rosen, S. Hensley, I.R. Joughin, F.K. Li, S.N. Madsen, E. Rodriguez, and R.M. Goldstein, "Synthetic aperture radar interferometry," *Proc. IEEE*, vol.88, no.3, pp.333–382, March 2000.
- [7] G. Ferraiuolo, F. Meglio, V. Pascasio, and G. Schirinzi, "DEM reconstruction accuracy in multichannel SAR interferometry," *IEEE Trans. Geosci. Remote Sens.*, vol.47, no.1, pp.191–201, Jan. 2009.
- [8] S. Sauer, L. Ferro-Famil, A. Reigber, and E. Pottier, "Three-dimensional imaging and scattering mechanism estimation over urban scenes using dual-baseline polarimetric InSAR observations at L-band," *IEEE Trans. Geosci. Remote Sens.*, vol.49, no.11, pp.4616–4629, Nov. 2011.
- [9] K.A. Camara De Macedo, et al., "Long-term airborne DInSAR measurements at X-and P-bands: A case study on the application of surveying geohazard threats to pipelines," *IEEE J. of Selected Topics in Applied Earth Observations & Remote Sensing*, vol.5, no.3, pp.990–1005, June 2012.
- [10] C. Wang, X. Mao, and Q. Wang, "Landslide displacement monitoring by a fully polarimetric SAR offset tracking method," *Remote Sensing*, vol.8, no.8, p.624, Aug. 2016.
- [11] R. Nakamata, R. Oyama, S. Kidera, and T. Kirimoto, "Accurate height change estimation method using phase interferometry of multiple Band-divided SAR images," *IEICE Trans. Commun.*, vol.E97-B, no.6, pp.1205–1214, June 2014.
- [12] Y. Yamaguchi, "Disaster monitoring by fully polarimetric SAR data acquired With ALOS-PALSAR," *Proc. IEEE*, vol.100, no.10, pp.2851–2860, Oct. 2012.
- [13] T. Moriyama, S. Uratsuka, T. Umehara, M. Satake, A. Nadai, H. Maeno, K. Nakamura, and Y. Yamaguchi, "A study on extraction of urban areas from polarimetric synthetic aperture radar image," *Geosci. & Remote Sensing IGRASS '04 Proc.*, vol.1, pp.703–706, Sept. 2004.
- [14] S. Hong, S. Wdowinski, and S. Kim, "Evaluation o TerraSAR-X

observation for wetland InSAR application," *IEEE Trans. Geosci. Remote Sens.*, vol.48, no.2, pp.864–873, Feb. 2010.

- [15] A. Marino, S.R. Cloude, and I.H. Woodhouse, "A Polarimetric target detector using the Huynen fork," *IEEE Trans. Geosci. Remote Sens.*, vol.48, no.5, pp.2357–2366, May 2010.



Ryo Oyama received his B.E. degrees in Electronic Engineering from University of Electro-Communications in 2013. He is currently studying M.E. degree at the Graduate School of Informatics and Engineering, University of Electro-Communications. His current research interest is advanced radar signal processing of SAR application.



Shouhei Kidera received his B.E. degree in Electrical and Electronic Engineering from Kyoto University in 2003 and M.I. and Ph.D. degrees in Informatics from Kyoto University in 2005 and 2007, respectively. He is currently an Associate Professor in Graduate School of Informatics and Engineering, the University of Electro-Communications, Japan. His current research interest is in advanced radar signal processing or electromagnetic inverse scattering issue for ultra wideband (UWB) sensor. He was awarded Ando Incentive Prize fo the Study of Electronics in 2012, Young Scientist's Prize in 2013 by the Japanese Minister of Education, Culture, Sports, Science and Technology (MEXT), and Funai Achievement Award in 2014. He is a member of the Institute of Electrical and Electronics Engineering (IEEE) and the Institute of Electrical Engineering of Japan (IEEJ).



Tetsuo Kirimoto received the B.S. and M.S. and Ph.D. degrees in Communication Engineering from Osaka University in 1976, 1978 and 1995, respectively. During 1978–2003 he stayed in Mitsubishi Electric Corp. to study radar signal processing. From 1982 to 1983, he stayed as a visiting scientist at the Remote Sensing Laboratory of the University of Kansas. From 2003 to 2007, he joined the University of Kitakyushu as a Professor. Since 2007, he has been with the University of Electro-Communications, where he is a Professor at the Graduate School of Informatics and Engineering. His current study interests include digital signal processing and its application to various sensor systems. Prof. Kirimoto is a senior member of IEEE and a member of SICE (The Society of Instrument and Control Engineers) of Japan.